


# Electromagnetic shielding effectiveness of 3D printed polymer composites

Z. Viskadourakis<sup>1</sup> · K. C. Vasilopoulos<sup>1</sup> · E. N. Economou<sup>1</sup> · C. M. Soukoulis<sup>1,2</sup> · G. Kenanakis<sup>1</sup> 

Received: 7 September 2017 / Accepted: 27 October 2017  
© Springer-Verlag GmbH Germany 2017

**Abstract** We report on preliminary results regarding the electromagnetic shielding effectiveness of various 3D printed polymeric composite structures. All studied samples were fabricated using 3D printing technology, following the fused deposition modeling approach, using commercially available filaments as starting materials. The electromagnetic shielding performance of the fabricated 3D samples was investigated in the so called C-band of the electromagnetic spectrum (3.5–7.0 GHz), which is typically used for long-distance radio telecommunications. We provide evidence that 3D printing technology can be effectively utilized to prepare operational shields, making them promising candidates for electromagnetic shielding applications for electronic devices.

## 1 Introduction

Nowadays, high-performance, high-processing electronic devices are used, to improve our everyday life, such as cell phones, wearable smart devices, microwave ovens, wireless communication systems, television and navigation systems, radar equipment, etc., to name just a few. These type of electronic devices definitely enhance the quality level of human lives; however, they also act as electromagnetic radiation emitters. Such electromagnetic emission perturbs

the function of other surrounding electronic devices, and even worse, it can introduce radiative damage of biological/living species [1]. This electromagnetic coupling, so called electromagnetic interference (EMI), mainly contributes to the enhancement of the so-known electromagnetic pollution.

Several attempts have been taken to address EMI issues, by developing materials that absorb or reflect electromagnetic radiation in a particular range of frequencies; these materials can be used as radiation shields for sensitive electronics, or even to protect human from radiation. Notably, an effective EMI shielding material is characterized by both high electric conductivity and high dielectric constant. Such properties are mostly found in metals [2], thus metallic thin foils and sheets are widely used as EMI shields. Although the effective shielding properties of metals are satisfactory, their processing cost is quite high and they are sensitive to corrosive environments [3, 4]; the latter is a main drawback for practical applications.

On the other hand, conducting nanostructured multilayers and composites have recently attracted interest for electromagnetic shielding applications, particularly in the GHz regime, since they exhibit advantages such as lightweight, corrosion resistance and low processing prices. Thus polymer composites with carbon-based inclusions (i.e., graphite, black carbon, carbon fibers, etc.) have been extensively studied as shielding materials [5–9]; graphene has also been investigated [10, 11]. Nevertheless, up to now, such carbon nanostructures have not been used in everyday applications, since several technical issues are pending, such as layer composition, growth methods and understanding of the underlying mechanisms.

Three-dimensional (3D) printing process has recently gained considerable interest, as an alternative way to fabricate polymers and polymeric nanocomposite materials [12]. Although several 3D printing techniques have been

✉ G. Kenanakis  
gkenanak@iesl.forth.gr

<sup>1</sup> Institute of Electronic Structure and Laser, Foundation for Research & Technology-Hellas, N. Plastira 100, 70013 Heraklion, Crete, Greece

<sup>2</sup> Ames Laboratory and Department of Physics and Astronomy, Iowa State University, Ames, IA 50011, USA

proposed, the fused deposition modeling (FDM)/fused filament fabrication (FFF) [13] method is the most appropriate for building 3D structures. In this method, the polymer melt extrudes out of a heated nozzle to form a 3D shape by layer-by-layer deposition on a platform. Common materials used as filaments in the FDM process are poly lactic acid (PLA), acrylonitrile butadiene styrene (ABS), polycarbonate (PC), polyvinyl alcohol (PVA), etc. Such materials are insulating; thus in pure form they cannot be used for EMI shielding applications. Nevertheless, carbon-based inclusions can be embedded (at least in some of them), enhancing their conductivity, and thus improving their EMI properties.

Preparation of shielding layers, consisting of polymer nanocomposites, using 3D printing technology exhibits several potential advantages in comparison to other methods. Traditionally, plain polymer layer formation takes place in chemical labs, using complex chemical routes and reagents, thus it is a complex and time consuming process. Furthermore, the construction of complex structural 3D patterns onto polymeric plain surfaces includes the use of expensive dedicated lithographic techniques, such as stereolithography and nano-imprinted lithography. On the other hand, 3D printed shielding layers can be produced in short time, while complex structures can be built, in a single-step process.

In this study we adopted the 3D printing technology to construct 3D structures, with improved EMI shielding performance. Several commercial available polymeric materials (ABS, PLA, etc.), along with polymer-based composites enriched with carbon nanostructures (nanotubes and nanofillers), in the form of cylindrical wires (known as 3D printer filaments) were used to build such 3D structures. Moreover, different 3D structures, comprising of the same building material, were also investigated, to verify their optimum EMI performance. In all cases, the structural, dielectric, and the electrical properties of the fabricated samples were also investigated. Some of them provided an efficient electromagnetic shielding performance, making them promising candidates for several electronics applications.

## 2 Experimental

### 2.1 Materials and 3D printed samples fabrication

Several commercially available filaments (1.75 mm diameter) suitable for 3D printing were used for the purposes of this study. Codes and nominal names are listed in Table 1; pure acrylonitrile butadiene styrene (ABS), conducting poly lactic acid (PLA) composite, doped with graphite, polymeric composite consisting of ABS and carbon nanotubes (CNT), and composite filament comprising of PLA and graphene oxide were studied. All filaments were carefully chosen, so

as they exhibit resistivity values varying in a wide range  $1\text{--}10^{-9}$   $\Omega$  cm.

A dual-extrusion FDM-type 3D printer (Makerbot Replicator 2X) was used for the direct fabrication of 3D structures. The FMD process of building a solid object involves heating of the fed filament and pushing it out layer-by-layer through a heated (210 °C) nozzle (0.4 mm inner diameter) onto a heated surface (50 °C), via a computer controlled three-axis positioning system (with a spatial resolution of approximately 100  $\mu\text{m}$  in  $z$ -axis and 11  $\mu\text{m}$  in  $x$  and  $y$ ). Following the approach above, several 3D printed samples were fabricated in a layer-by-layer fashion, with each layer fixed at 0.2 mm, and the filling factor at 100%, indicating that all samples are fully packed. Filling pattern is kept linear and the pattern of each layer is rotated by 90°, with respect to the neighbor layers. For each filament used in printing, two types of samples were being built, one parallelepiped with flat surfaces (21 mm  $\times$  47 mm  $\times$  1 mm), and another with pyramids printed in one side. Each pyramid has rectangular base (2.5 mm  $\times$  2.5 mm) and its height being 2.5 mm. One representative geometry, along with the dimensions of the 3D printed samples with pyramids, is schematically shown in Fig. 1.

### 2.2 Characterization

#### 2.2.1 Optical and electron microscopy measurements

The surface morphology of all the samples was determined using a typical optical microscope equipped with a 2 $\times$  objective lens and a WF10 $\times$  microscope wide field plane-scope eyepiece, under top illumination, providing a total magnification of 20 $\times$ , and a field emission scanning electron microscope (FE-SEM, JEOL JSM-7000F) with a magnification of 60 $\times$ .

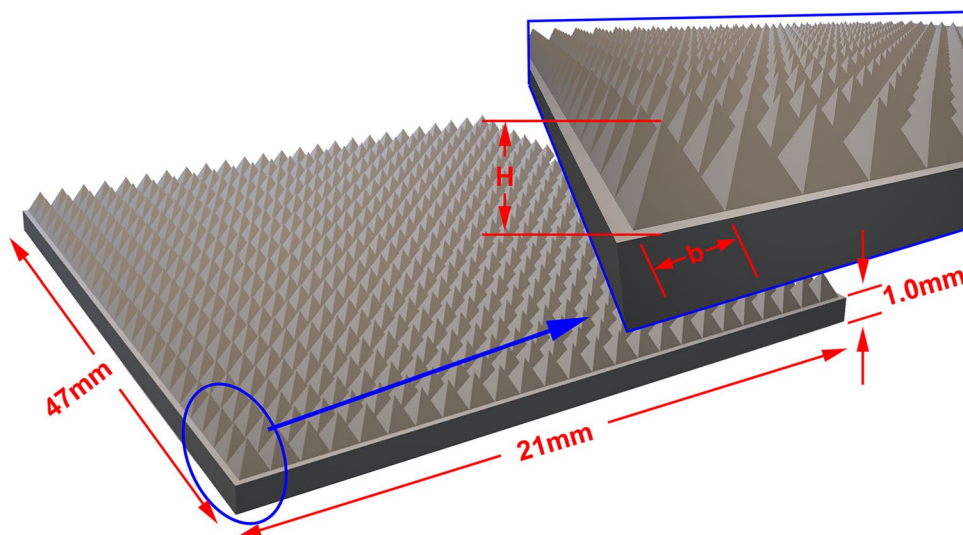
#### 2.2.2 X-ray diffraction experiments

The crystal structures of all the samples was determined by X-ray diffraction (XRD) experiments, using a Rigaku (RINT 2000) diffractometer with Cu  $K_{\alpha}$  ( $\lambda = 1.5406$  Å) X-rays for  $2\theta = 10.00^{\circ}$ – $60.00^{\circ}$  and a step time of 60°/s.

#### 2.2.3 Dielectric spectroscopy

Impedance spectroscopy measurements were performed for all samples, using a precision LCR bridge, in the frequency range 1.0 kHz–1.0 MHz. Samples under investigation were placed between two metallic plates forming a capacitor. An AC voltage was applied to the capacitor, and both the impedance  $Z$  and the angle  $\theta$  were measured. Both the dielectric permittivity  $\epsilon'$  and the dielectric loss  $D = \epsilon''/\epsilon'$  were

**Fig. 1** Representative image for 3D printed composite slabs studied. In the inset, one can see a magnified picture of the pyramid structure



then extracted. All measurements were performed at room temperature.

#### 2.2.4 Electrical resistivity

Two-probe resistivity measurements were performed in conductive samples, where applicable. Metallic contacts were being developed on the samples, using conducting silver paste. Copper wires were attached on the silver paste contacts, the other end of which, were connected on a Keithley 2400 Source Measure Unit (SMU). DC voltage sweeps were applied, while current was recorded, so as  $I$ - $V$  curves were being produced. All measurements were performed at room temperature.

### 2.3 Electromagnetic induction shielding efficiency (EMI SE) measurements

Electromagnetic induction shielding measurements (reflection and transmission coefficients,  $S_{11}$  and  $S_{21}$ , respectively) were measured using a Hewlett-Packard 8722 ES Vector Network Analyzer (VNA). The rectangular samples ( $25 \times 13 \times 1.2$  mm) of printed structures were inserted into a WR-187 rectangular waveguide (frequency range 3.5–7.0 GHz) and they were placed between the two ports of the network analyzer.

## 3 Results and discussion

### 3.1 Surface morphology

Figure 2 depicts an optical microscopy picture along with an SEM photograph of an ABS 3D printed pyramid. The 3D structure of the printed samples can be clearly seen from

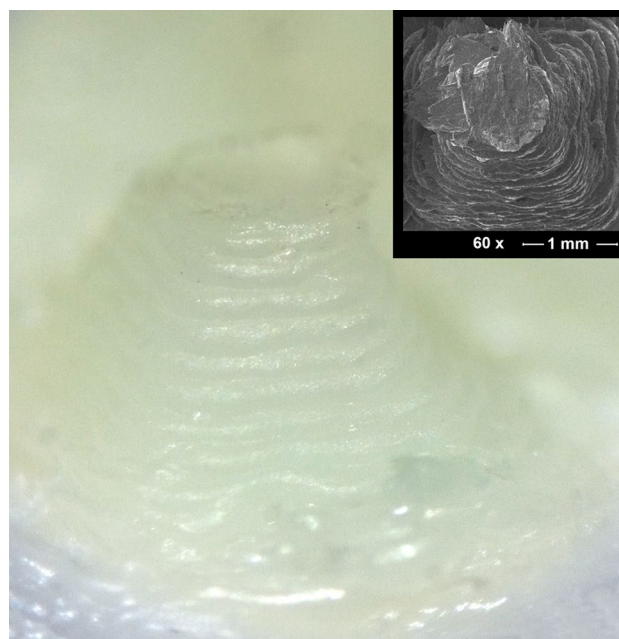


**Fig. 2** Optical microscopy and SEM (inset) picture of an ABS 3D printed pyramid

Fig. 2, resembling a truncated pyramid, instead of a typical square pyramid. Moreover, one can see from Fig. 2 the layer-by-layer fabrication of the 3D printed samples, with a  $\sim 100$   $\mu\text{m}$  spatial resolution in  $z$ -axis, as already reported in the experimental part of this manuscript.

### 3.2 XRD patterns

Figure 3 shows a typical X-ray diffraction pattern of CON-GRA sample, verifying its crystalline properties. The XRD pattern depicts typical peaks of the PLA profile [14] and all

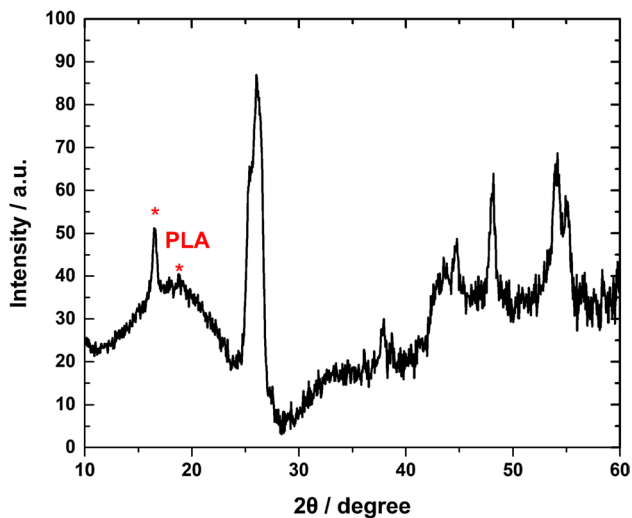


**Fig. 3** Typical XRD pattern of CON-GRA samples. Intensity peaks of the PLA polymer matrix marked with asterisks. Corresponding XRD spectra were taken for all studied samples (not shown here)

the characteristic diffraction peaks of graphite, according to the JCPDS card, No. 75-1621 [15, 16]. Correspondingly all XRD spectra taken for all studied samples (not shown here) exhibit peaks concerning the carbon structures inclusions (present in our samples) and peaks regarding to the polymeric matrix.

### 3.3 Dielectric spectroscopy

Dielectric permittivity  $\epsilon'$  and dissipation factor  $D = \tan\delta = \epsilon''/\epsilon'$  of fabricated samples is shown in Fig. 4. Dielectric permittivity for CON-GRA, cannot be determined due to its high electrical conductivity. Nevertheless, ABS, CNT001 and CON-PLA show a typical dielectric behavior, as a function of frequency. Specifically, both ABS and CNT001 exhibit typical low  $\epsilon'$  and  $D$  values. On the other hand, CON-PLA exhibits high  $\epsilon'$  as well as high  $D$  values. Increased  $\epsilon'$  values are attributed to the polar characteristics of carbon inclusions, which enhance the number of charge carriers in the polymeric matrix. The increased  $\tan\delta$  is connected to the fact that the conductivity of the composite increases as well. In the case of the CON-PLA sample, the conductivity is quite significant, giving rise to the enhancement of the  $\tan\delta$  above 1, indicating high dielectric losses.

### 3.4 Electrical resistivity

DC resistivity values, of all studied 3D printed samples are presented in Table 1. Resistivity of 3D printer filaments, used for building the samples, is also shown for direct comparison. ABS is a typical insulator, showing an unmeasurable resistivity. However, polymeric composites including

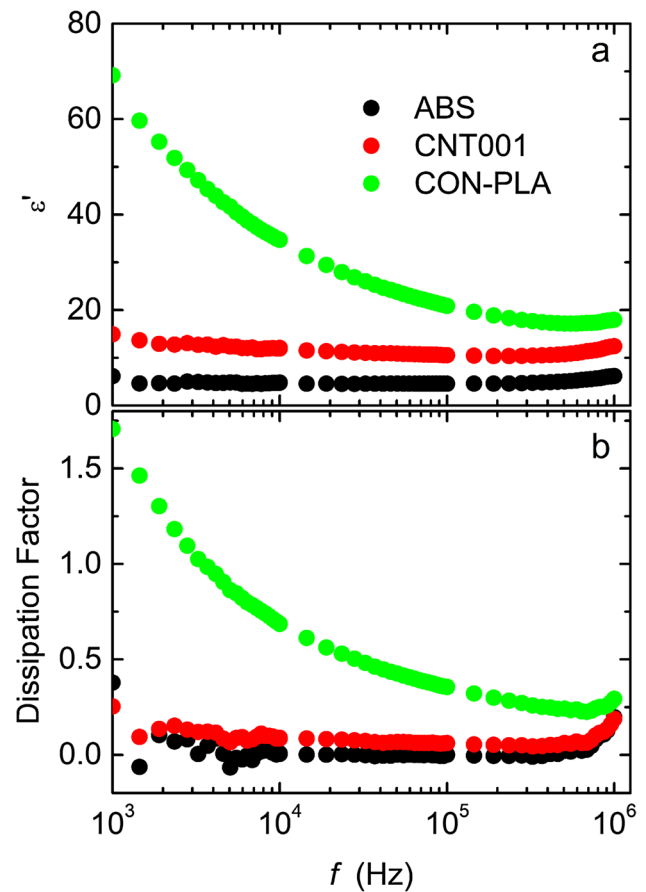


**Fig. 4** Real part of the dielectric permittivity (a), and dissipation factor as a function of frequency (b), for ABS (black solid circles), CNT001 (red solid circles) and CON-PLA (green solid circles), respectively. Dielectric loss dramatically increases for conductive composites, such as CON-PLA

various types of carbon show varying resistivity values. In particular, CON-GRA is the most conductive among all samples, while conductive CON-PLA sample shows resistivity value comparable to the CON-GRA. CNT001 composite shows higher resistivity values.

Comparing the resistivity of the samples to those of the filament we found mixed results. In particular, CNT001 3D printed samples show lower resistivity values in comparison to their corresponding filaments. On the other hand, both CON-PLA and CON-GRA samples exhibit higher resistivity than the corresponding filaments. The electrical resistivity is obviously affected by the printing process. In general, conductive filaments consist of an insulating polymer matrix in which conductive inclusions are embedded. These inclusions are distributed into the polymer and percolate in such a way that a conductive path is formatted resulting to their macroscopic high electrical conductivity (or low resistivity). Obviously, both the concentration and the distribution of the inclusions into the polymeric matrix affect considerably their



**Table 1** Code names, compositions and resistivity values for all filaments used for 3D printing, as well as for all samples studied

Code name	Sample	Filament’s volume resistivity ( $\Omega$ cm)	Sample’s volume resistivity ( $\Omega$ cm)
ABS	Pure ABS	– <sup>a</sup>	– <sup>a</sup>
CNT001	ABS + carbon nanotubes	– <sup>a</sup>	$(67.2 \pm 0.1) \times 10^3$
CON-PLA	PLA + graphite	$4.72 \pm 0.05$	$9.75 \pm 0.05$
CON-GRA	PLA + graphene	$0.855 \pm 0.002$	$2.38 \pm 0.01$

<sup>a</sup>The resistivity values for these filaments/samples could not be measured using a Keithley 2400 Source Measure Unit (SMU)

physical properties, i.e., their resistivity [17]. The inclusion dispersity could be modified by the printing parameters such as printing speed, nozzle temperature, etc. Under optimized printing conditions the dispersion of the inclusions into the polymer matrix slightly changes, resulting to a 3D printed sample exhibiting properties similar or even better than the used filament. In other cases a general degradation of the polymer [18 and references therein] occurs, which further affects negatively the electrical resistivity of the produced sample. It must be noted that this is a plausible scenario to interpret the resistivity data among 3D samples and the corresponding filaments used. Nevertheless, in our case, it is not fully supported by experimental evidence since there is not any direct information regarding the dispersion of the inclusions into the polymer matrix and how it is changed after the printing process. It would be of great importance, to clarify the effect of the printing parameters on the electrical properties of a 3D printed sample; however, it is probably beyond the aims of the current study.

### 3.5 Electromagnetic shielding

When an electromagnetic field is incident on a surface, a part of the incident field is absorbed by the material, another part is reflected and the rest is transmitted through the material, as power balance dictates:

$$T + R + A = 1, \tag{1}$$

where  $T$ ,  $R$  and  $A$  are the transmission, reflection and absorption power counterparts, respectively. In materials of high electromagnetic shielding performance the transmission of the incident electromagnetic field, beyond the shielding material, is ideally zero. Hence, the incident field is either absorbed within the shielding material or reflected from it. The electromagnetic shielding performance can be effectively described by the EMI shielding effectiveness (SE). SE (also denoted as  $SE_T$ , with T indicating the transmission) is usually quantified in terms of the logarithm of the incident power  $P_{inc}$  over the transmitted power  $P_{trn}$  [19, 20] and it is expressed in decibels (dB). Thus, an effective shielding material absorbs or reflects a great part of the incident radiation, resulting to high dB levels of EMI.

$$SE = SE_T \ 10\log_{10}\left(\frac{P_{inc}}{P_{trn}}\right) = 10\log_{10}\left(\frac{1}{T}\right) = SE_R + SE_A, \tag{2}$$

where

$$SE_R = 10\log_{10}\left(\frac{1}{1 - R}\right), \tag{3}$$

and

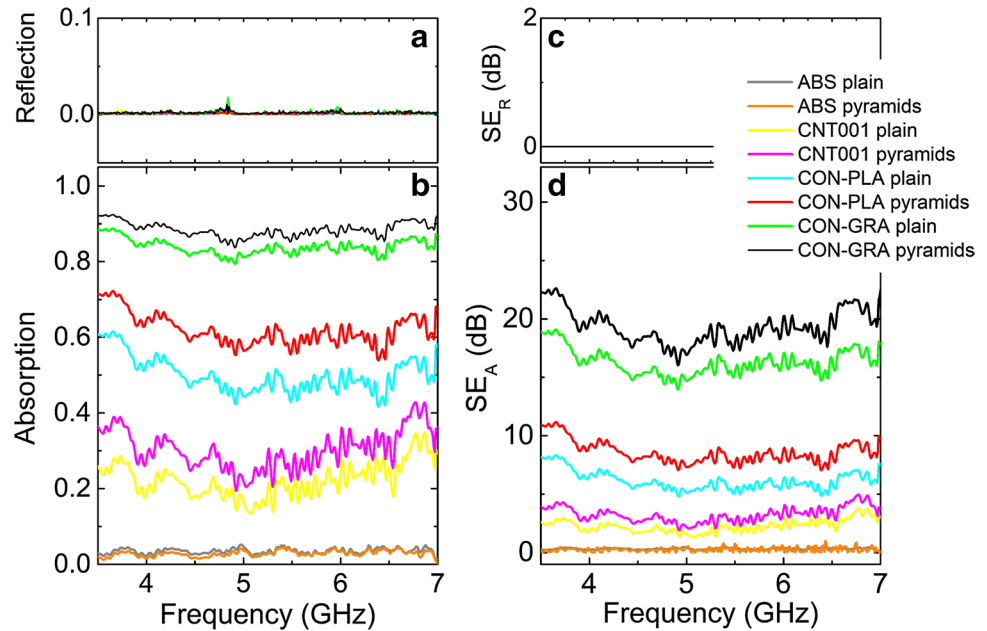
$$SE_A = 10\log_{10}\left(\frac{1 - R}{T}\right) \tag{4}$$

$SE_R$ ,  $SE_A$  refer to the reflection and absorption SE, respectively.

Figure 5 shows both the reflection (Fig. 4a) and the absorption (Fig. 5b) spectra of the studied 3D structures in the range 3.5–7.0 GHz. It is clearly shown that reflection of all studied specimens is nearly zero, resulting to the almost negligible the EMI shielding ( $SE_R$ ) effect due to reflection (Fig. 5c). Thus, absorption is the dominant shielding mechanism, i.e., total SE is reduced to  $SE_T = SE_A$ . On the other hand, absorption is obviously affected by the type of the filament, used for 3D printing. In particular ABS samples do not absorb, while CNT001 samples exhibit low absorption levels, resulting to low  $SE_A$  values, as well (Fig. 5d). Nonetheless, CON-PLA absorbs above 50% while CON-GRA samples efficiently absorbs, up to 90%. Notably both of them exhibit high conductivity values. Correspondingly  $SE_A$  levels for CON-PLA is approximately 10 dB while for the CON-GRA is ~20dB, in the whole measured frequency range.

Furthermore, it is seen that the absorption is also affected by the landscape of the sample; for all samples, on the surface of which pyramids have been grown, absorption is enhanced, in comparison to the plain surface samples. Nonetheless, during pyramid growth on the plain surfaces, excess material is used; hence the mass of the sample increases. Consequently, the natural question arising is whether the better shielding performance is due to the pyramid structures or it is just a mere mass effect. All plain samples studied here, exhibit an area of 987 mm<sup>2</sup>. Each pyramid, on the other hand, has an area of ~14 mm<sup>2</sup>.

**Fig. 5** Reflection (a) and absorption (b) spectra from 3.5 to 7.0 GHz (C-band) for all studied samples. The electromagnetic interference shielding effect due to reflection  $SE_R$  (c), as well as absorption  $SE_A$  (d) are also pictured. The effect of pyramid structure is also shown in both absorption and  $SE_A$  graphs



Each plain sample can accommodate 144 pyramids, thus the total surface increases to  $\sim 2016 \text{ mm}^2$ , i.e.,  $\sim 104\%$  increment. Additionally, the weight of the pyramid-structured samples increases by  $\sim 60\%$  compared to the plain ones, resulting to a  $\sim 26\%$  increment of the corresponding area-to-weight ratio. If we compare the absorption spectra of plain and pyramid-structured samples, we can notice it increases (for the case of pyramids), in average, by  $\sim 35$ ,  $\sim 15$  and  $\sim 5\%$  for CNT001, CON-PLA and CON-GRA, respectively. Furthermore, as far as the shielding efficiency concerned, it also increases (in average) by  $\sim 50$ ,  $40$  and  $20\%$  for CNT001, CON-PLA and CON-GRA, correspondingly. It is obviously seen that the shielding performance of the pyramid-structured samples is not related to the area-to-weight ratio increment. Moreover, considering that the resistivity of the CNT001 is three orders of magnitude higher than both the CON-PLA and CON-GRA samples, it could be safely if concluded that in low resistivity (or highly conductive) samples the presence of pyramids slightly affects their shielding performance. In contrast, pyramid structures significantly affect the shielding properties of the high resistivity (or low conductive) samples.

Comparing to results reported here with that of other 3D printed polymer composites [13, 21, 22] we conclude that CON-GRA exhibits more efficient EMI shielding properties. In any case, a SE level higher than  $\sim 15 \text{ dB}$  is required for commercial shielding applications, and thus CON-GRA becomes a good candidate for EMI shielding applications. On the other hand CON-PLA is promising for such applications, although still needs to be improved.

### 3.6 Summary and conclusion

In summary, we studied the EMI shielding properties of several 3D printed polymeric composite structures. 3D printing technology provides significant advantages in producing electromagnetic shielding layers, since it is a quick, single-step method to build complex 3D structures and patterns. Various commercially available filaments were used to build such 3D structures. XRD was utilized to confirm the crystal structure of the studied materials, while electrical resistivity was also measured, showing that carbon included polymer composites exhibit higher conductivity than pure polymer samples. Dielectric permittivity measurements revealed the enhancement of the dielectric losses as the conductivity of the 3D printed structure increases. EMI performance was investigated in the so called C-band of the electromagnetic spectrum (3.5–7.0 GHz), which is typically used for long-distance radio telecommunications. It is shown that 3D printed graphene-based samples exhibit efficient electromagnetic shielding performance, making them promising candidates for several electronics applications. Furthermore, we emphasize that altering the 3D geometry of the samples (e.g., by building pyramids, a process rather trivial in the framework of our approach) the EMI shielding efficiency can be considerably enhanced, especially in samples with low conductivity. The above argument can be utilized in general for high resistivity (or low conductive) samples to enhance their shielding performance. In conclusion, it is shown that 3D printing technology can be effectively utilized to prepare EMI effective shields, using commercially

available filaments, which consist of carbon nanostructures, such as nanotubes or nanofillers in a polymeric matrix.

**Acknowledgements** This work was supported by the European Research Council under ERC Advanced Grant no. 320081 (PHOTO-META). Work at Ames Laboratory was partially supported by the Department of Energy (Basic Energy Sciences, Division of Materials Sciences and Engineering) under Contract no. DE-AC02-07CH11358. Financial support by the EU-FET Graphene Flagship (Grant agreement no: 604391) is also acknowledged.

## References

1. L. Hardell, C. Sage, *Biomed. Pharmacother.* **62**, 104 (2008)
2. S. Celozzi, R. Araneo, G. Lovat, in *Wiley Encyclopedia of Electrical and Electronics Engineering* (Wiley, New York, 2008), p. 1, 4, 42
3. X. Tong, in *Advanced Materials and Design for Electromagnetic Interference Shielding* (CRC Press, Taylor & Francis Group LLC, Boca Raton, 2009), p. 132
4. D.C.T.S. Geetha, K.K. Satheesh Kumar, R.K. Chepuri, M. Rao, Vijayan, *J. Appl. Polym. Sci.* **113**, 2073 (2009)
5. Y. Yang, M.C. Gupta, K.L. Dudley, R.W. Lawrence, *J. Nanosci. Nanotechnol.* **5**, 927 (2005)
6. P.C.P. Watts, W.K. Hsu, H.W. Kroto, D.R.M. Walton, *Nano Lett.* **3**, 549 (2003)
7. H.M. Kim, K. Kim, C.Y. Lee, J. Joo, S.J. Cho, H.S. Yoon, D.A. Pejaković, J.W. Yoo, A.J. Epstein, *Appl. Phys. Lett.* **84**, 589 (2004)
8. Y. Yang, M.C. Gupta, K.L. Dudley, R.W. Lawrence, *Nano Lett.* **5**, 2131 (2005)
9. G. Kenanakis, K.C. Vasilopoulos, Z. Viskadourakis, N.-M. Barkoula, S.H. Anastasiadis, M. Kafesaki, E.N. Economou, C.M. Soukoulis, *Appl. Phys. A* **122**, 802 (2016)
10. Y. Yang, M.C. Gupta, K.L. Dudley, *Nanotechnology* **18**, 345701 (2007)
11. M.S. Kim, J. Yan, K.H. Joo, J.K. Pandey, Y.J. Kang, S.H. Ahn, *J. Appl. Polym. Sci.* **130**, 3947 (2013)
12. C.R. Rocha, A.R. Torrado Perez, D.A. Roberson, C.M. Shemelya, E. MacDonald, R.B. Wicker, *J. Mater. Res.* **29**, 1859 (2014)
13. K. Prashantha, F. Roger, *J. Macromol. Sci. Part A Pure Appl. Chem.* **54**, 24 (2017)
14. E.D.M. Teixeira, A. de Campos, J.M. Marconcini, T.J. Bondancia, D. Wood, A. Klamczynski, L.H.C. Mattoso, G.M. Glenn, *RSC Adv.* **4**, 6616 (2014)
15. R. Zhang, Y. Liu, L. Yu, Z. Li, S. Sun, *Nanotechnology* **24**, 225601 (2013)
16. J.Y. Howe, C.J. Rawn, L.E. Jones, H. Ow, *Powder Diffr.* **18**, 150 (2003)
17. M. Šupová, G.S. Martynková, K. Barabaszová, *Sci. Adv. Mater.* **3**, 1 (2011)
18. K. Gnanasekaran, T. Heijmans, S. van Bennekom, H. Woldhuis, S. Wijnia, G. de With, H. Friedrich, *Appl. Mater. Today* **9**, 21 (2017)
19. M.H. Al-Saleh, W.H. Saadeh, U. Sundararaj, *Carbon N. Y.* **60**, 146 (2013)
20. M.H. Al-Saleh, U. Sundararaj, *Compos. Part A Appl. Sci. Manuf.* **42**, 2126 (2011)
21. R. Kotsilkova, E. Ivanov, P. Todorov, I. Petrova, N. Volynets, A. Paddubskaya, P. Kuzhir, V. Uglov, I. Biró, K. Kertész, G.I. Márk, L.P. Biró, *J. Appl. Phys.* **121**, 063102 (2017)
22. A. Paddubskaya, N. Valynets, P. Kuzhir, K. Batrakov, S. Maksimenko, R. Kotsilkova, H. Velichkova, I. Petrova, I. Biró, K. Kertész, G.I. Márk, Z.E. Horváth, L.P. Biró, *J. Appl. Phys.* **119**, 135102 (2016)